A DFT-Based Theoretical Investigation of the Mechanism of the $PtCl_2$-Mediated Cycloisomerization of Allenynes

Elena Soriano*[a] and José Marco-Contelles[b]

Abstract: The mechanism of Pt^{II}-catalyzed intramolecular cycloisomerization of allenyne systems has been extensively investigated by DFT calculations. Different mechanistic schemes have been proposed and discussed, including the Alder–ene reaction. The free energy results suggest that the kinetically preferred reaction pathway for precursors that are tri- and tetrasubstituted on the allene moiety should proceed by a five-step mechanism. This would involve formation of a platina(IV)cyclopentene intermediate by selective engagement of the external π bond of the allene, which would undergo regioselective β-H elimination from the equatorially disposed methyl group. A metal-induced H migration leads to a second octahedral Pt^{IV}–chelate complex, which would yield the expected bicyclic system through an intramolecular migratory insertion step. Therefore, depending on the conformation of the initial η^4-reactant complex for trisubstituted patterns, two possible intermediates can be formed that would evolve through different paths. In these cases, the regio- and stereochemical outcomes predicted by the mechanistic scheme proposed agree with experimental data. Substituted precursors on the alkyne moiety follow a distinct, four-step, mechanism also involving an oxidative cyclometalation process to an octahedral Pt^{IV} intermediate complex. Theoretical results reveal the kinetic preference for β-H elimination from the allylic group rather than from the *gem*-dimethyl group, which should account for the observed regioselectivity.

Keywords: cyclization · density functional calculations · metallacycles · reaction mechanisms · regioselectivity

Introduction

In recent years, the development of new synthetic methodologies mediated by transition-metal complexes has provided a variety of possibilities for the efficient preparation of organic molecules. Numerous studies have shown that $PtCl_2$ catalyzes the intramolecular skeletal rearrangement of 1,6-enynes to afford different types of cycloadducts.[1] Theoretical mechanistic analyses have revealed that many of these reactions proceed through cyclopropyl platinum–carbene intermediates formed by initial 5-*exo* or 6-*endo*-cyclization steps.[2] Alternatively, simultaneous coordination of $PtCl_2$ to the alkyne and alkene moieties promotes the formation of Alder–ene products through oxidative cyclometalation.[2b]

On the other hand, allenyne systems may also undergo transition-metal-catalyzed intramolecular cycloisomerization reactions. For instance, Wilkinson's catalyst ($[RhCl(PPh_3)_3]$),[3] $[(\eta^2\text{-propene})Ti(O\text{-}iPr)_2]$,[4] and the complex $[CpCo(CO)_2]$[5] catalyze the ene-type cycloisomerization of 1,7-allenynes to give cross-conjugated trienes. Additionally, it has been reported that allenynes can exhibit different modes of cyclization depending on the metallic catalyst: Pd complexes catalyze cyclization of 1,7-allenynes to six-membered carbocyles, whereas Rh complexes afford five-membered rings.[6] Interestingly, in spite of this and related efforts on this subject,[7–11] it was only very recently that Brummond et al. established that substitution of the allene has an influence on the regiochemical course of this reaction.[12]

We have started a project aimed at the DFT-based investigation of the mechanisms of transition-metal-promoted processes for different types of unsaturated substrates to ra-

[a] Dr. E. Soriano
Sección de Síntesis Orgánica e Imagen Molecular por Resonancia Magnética
Instituto Universitario de Investigación, UNED
Facultad de Ciencias
C/Senda del Rey, 9, 28040 Madrid (Spain)
Fax: (+34) 913-986-697
E-mail: esoriano@arrakis.es

[b] Prof. J. Marco-Contelles
Laboratorio de Radicales Libres
Instituto de Química Orgánica General (CSIC)
C/Juan de la Cierva 3, 28006 Madrid (Spain)

Supporting information for this article is available on the WWW under http://www.chemeurj.org/ or from the author.

 DOI: 10.1002/chem.200400618

tionalize the reported experimental data in terms of chemo-, regio-, and stereoselectivity. In this context, we have carried out theoretical studies on cycloisomerization mechanisms, with or without skeletal reorganization, of 1,6-enynes, heteroatom-tethered enynes, unsaturated propargylic carboxylates, or dienynes.[13]

Herein we report a detailed theoretical study on the elucidation of the reaction pathways for the $PtCl_2$-mediated cycloisomerization of substituted allenynes. The experimental results recently reported[14] have revealed a clear dependence of cycloisomerization products upon the substitution on allene and alkyne moieties (Scheme 1). Based on these

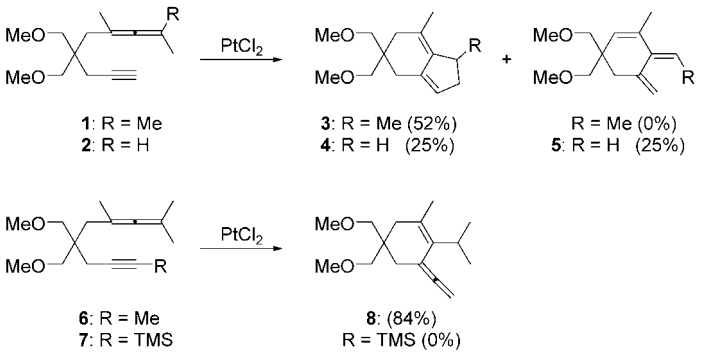

Scheme 1. $PtCl_2$-mediated cyclization of allenynes.

observations, we have explored the possible mechanism(s) involved to gain a deeper understanding of these processes. A detailed knowledge of the factors that control the evolution of key intermediate structures would allow us to carry out more efficient and selective cycloisomerization reactions to afford important carbocyclic skeletons.

We have chosen compounds **9**–**11** as theoretical models to simplify our analysis of the potential energy surfaces (PES).

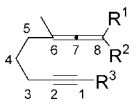

9: $R^1=R^2=CH_3$; $R^3=H$
10: $R^1=CH_3$; $R^2=R^3=H$
11: $R^1=R^2=R^3=CH_3$

Results and Discussion

Substitution on the terminal carbon atom of allene: Formation of the bicyclo[4.3.0]nonane ring system **3** (Scheme 1) suggests that initial cyclization takes place selectively with the external π bond of the allene. In analogy with the mechanistic scheme proposed by Echavarren and co-workers[2b] for the Alder–ene reaction of enynes, these processes might also involve a platinacyclopentene as the key intermediate (structure **B**, Scheme 2). Interestingly, a homologous metallabicyclic structure was identified in Ti^{II}-mediated allenyne cyclizations.[15] Hence, we have analyzed the reaction pathway involving the formation of **B** through an initial intramolecular oxidative cyclization of reactant complex **A** (Scheme 2). Subsequent β-H elimination, 5-*endo* carboplatination, and reductive elimination steps would then afford the bicyclic adduct (Scheme 2, path **Ia**). As an alternative, a mechanistic scheme involving an intramolecular migratory insertion from a second platina(IV)cycle structure could also be envisaged (Scheme 2, path **Ib**).

On the basis of the results calculated for Pt^{II}-catalyzed cyclization of enynes,[13] an initial coordination of the alkyne to the metal center (structure **A′**, Scheme 2) could promote the intramolecular addition on one olefinic carbon atom to give the allylic carbocation intermediate **F**, which then could drive the reaction over to metallabicycle **B**. Nevertheless, this route was ruled out as a feasible pathway since it led to a strange cyclopropyl Pt-carbene intermediate (C1–C2 1.406, C1–C7 1.654, C2–C7 1.580, Pt–C8 1.933 Å) that did not show the expected allylic cation nature of the hypothetical structure **F**. The methyl groups in the terminal position of the allene, C8, do not lie on the same plane as substituent at C6 (50.3–67.0°). Furthermore, this structure cannot evolve to the projected intermediate in a subsequent step and it represents a dead end in the reaction pathway.

In contrast, coordination of both terminal π bonds of the allene and alkyne moieties with $PtCl_2$ forms the η^4-complex **React** (structure **A**, Scheme 2). The Pt–alkyne interaction (Pt–C1 2.187, Pt–C2 2.286 Å, Table S1, see Supporting Information) is slightly stronger than the Pt–allene interaction (Pt–C7 2.153, Pt–C8 2.373 Å) for the tetrasubstituted allene, with the Pt–terminal alkyne carbon atom and Pt–C7 distances being shorter than Pt–internal alkyne carbon atom and Pt–terminal allene carbon atom distances, respectively, due to steric factors. C1–C2 (1.242 in **A** compared to 1.208 Å in uncomplexed allenyne) and C7–C8 (1.380 compared to 1.313 Å in uncomplexed allenyne) bond lengthening clearly imply significant back-donation to the π* orbital of both unsaturated moieties. A regioselective cyclometalation step affords the platinacyclopentene intermediate **INT1** (structure **B**, Scheme 2) through the transition state **TS1** (Figure 1). This transition structure shows the incipient formation of the C2–C7 bond (2.123 Å), which involves a simultaneous increase in the Pt–C2 (2.632 Å) length and a strengthening of the Pt–C1 bond (2.051 Å). On the contrary, the Pt–allene interaction is stronger than in the reactant complex (Pt–C7 2.104 and Pt–C8 2.256 Å).

The complete formation of the C2–C7 bond (1.516 Å) takes place in the intermediate **INT1**, which shows a clear allylic structure since substituents at C8 are nearly coplanar to those at C6 (C6-C7-C8-C9 4.5°). This η^3 complex shows a C7–C8 bond longer (1.485 Å) than C6–C7 (1.398 Å) due to an interaction with the metal center (Pt–C8 2.165, Pt–C7 2.297, and Pt–C6 3.137 Å). The allylic bond angle (C6-C7-C8 128.1°) is larger than expected in order to relieve the steric congestion between methyl groups. Formation of **INT1** is exothermic ($\Delta G_{298} = -8.58$ kcal mol^{-1}, Table 1) and proceeds with a moderate activation energy ($\Delta G_{298}^{\neq} = 16.39$ kcal mol^{-1}), a value lower than that found for homologous enynes (ca. 30 kcal mol^{-1}).[2b,13a]

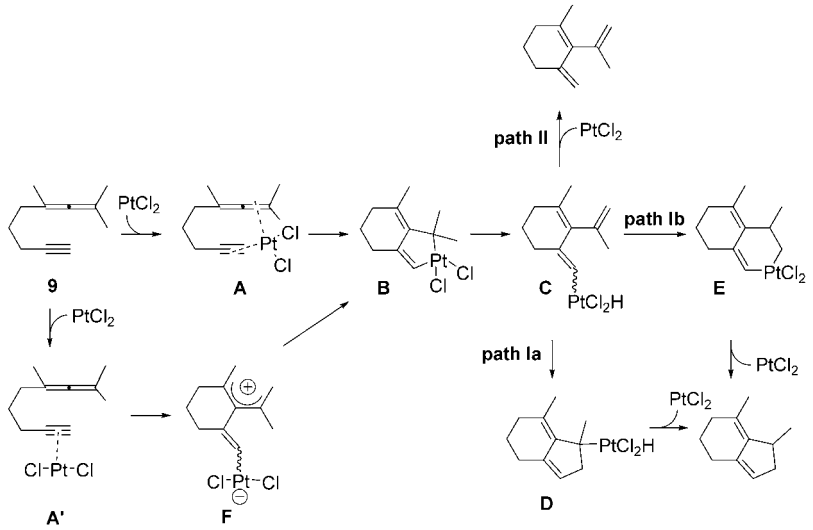

Scheme 2. Proposed mechanisms for the $PtCl_2$-catalyzed cyclization of allenynes.

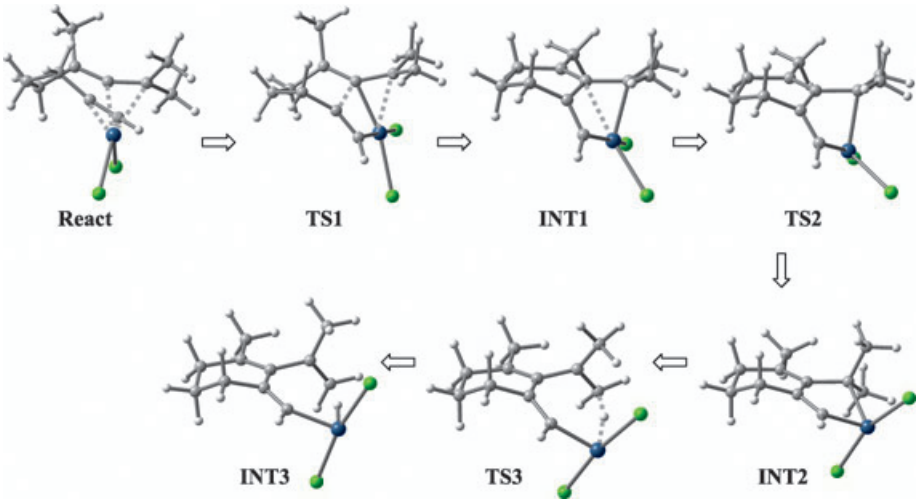

Figure 1. Optimized structures of $PtCl_2$-mediated intramolecular cycloisomerization of **9** (formation of **INT3**).

Table 1. Electronic[a] and free[b] energies computed for the $PtCl_2$-catalyzed intramolecular cycloisomerization of **9**.

	E[a] [a.u.]	G_{298}[b] [a.u.]	ΔE [kcal mol^{-1}]	ΔG_{298} [kcal mol^{-1}]
React	−1468.106766	−1468.152019	0.00	0.00
TS1	−1468.081058	−1468.125894	+16.13	+16.39
INT1	−1468.122032	−1468.165693	−9.58	−8.58
TS2	−1468.121739	−1468.164779	−9.40	−8.01
INT2	−1468.153555	−1468.197479	−29.36	−28.53
TS3	−1468.127432	−1468.171853	−12.97	−12.45
INT3	−1468.132822	−1468.178732	−16.35	−16.76
TS4a	−1468.105292	−1468.150188	+0.92	+1.15
TS4b	−1468.104638	−1468.152948	+1.34	−0.58
INT4a	−1468.135372	−1468.179814	−17.95	−17.44
INT4b	−1468.119266	−1468.164430	−7.84	−7.79
TS5a	−1468.081240	−1468.126701	+16.02	+15.89
TS5b	−1468.114266	−1468.158475	−4.71	−4.05
INT5a	−1468.132723	−1468.177745	−16.29	−16.14
TS6a	−1468.130344	−1468.173244	−14.80	−13.32
Prod	−1468.187904	−1468.230772	−50.91	−49.42

[a] Includes ZPE correction. [b] Includes thermal corrections at 298 K.

In a previous theoretical study concerning cycloisomerization of enynes, we observed that coordination of both alkene and alkyne moieties with $PtCl_2$ evolves by an oxidative cyclometalation step to afford an octahedral Pt^{IV} complex [Figure 2a] as the first intermediate structure.[13a] Conversely, the allylic nature in the intermediate Pt^{II} structure **INT1** formed in the first step for allenyne cycloisomerization does not have the same disposition; it shows square-planar coordination where the alkenyl ligand is placed in the coordination plane whereas the allylic moiety lies above it, and one of the *cis* chloride ligands is arranged *trans* to the σ-alkenyl bond [Figure 2b].

This structural motif has an important effect in the course of the process. We have noted that a proper disposition between the proton and metal acceptor orbital is essential for the β-H elimination step to proceed. Nevertheless, H on both methyl groups at C8 (C9 and C10) cannot lie on the same plane of the acceptor orbital.[13a] To overcome this apparent discrepancy, we proposed an additional step involving a metal

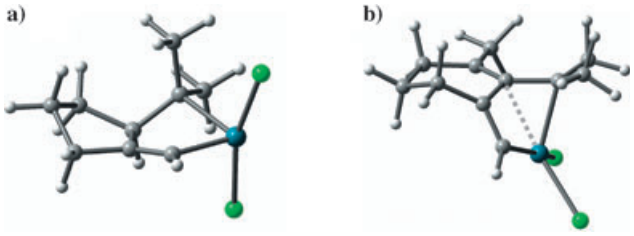

Figure 2. Comparison between metallacyclopentene structures formed from a) an enyne and b) allenyne precursors in the first step.

fragment rearrangement to afford the proper structure, namely, formation of the chelate complex **INT2** with a *trans* chloride ligand disposition (Figure 1).

This step takes place through the early transition structure **TS2**, which shows the incipient opening of the Cl-Pt-Cl bond angle (108.6°) and lengthening of the Pt−C7 interaction (2.421 Å). Harmonic frequency analysis of this transi-

tion state gives the unscaled imaginary frequency of $-49.1\ cm^{-1}$, indicating the rather small geometric distortion to reach it. These results agree with the low activation barrier computed for this elementary step ($0.57\ kcal\,mol^{-1}$, $-8.01\ kcal\,mol^{-1}$ relative to **React**, Table 1), which suggests that **INT1** should have a very transient life.

The subsequent intermediate Pt^{IV} complex **INT2** displays octahedral coordination of the ligands around the metal center with a *trans* arrangement of the chloro ligands (Cl-Pt-Cl 162.7°). This involves both Pt–Cl bond lengths and the NPA charge on the Cl ligands becoming similar (Tables S1 and S2, see Supporting Information). Consequently, there is a lower negative charge at C1 (−0.347 in **INT1** compared to −0.237 in **INT2**), which results from the less efficient π back bonding interaction with the metal. Our calculations indicate that formation of the metallacyclopentene **INT2** is favored from a thermodynamic viewpoint both in terms of the elementary step ($-19.95\ kcal\,mol^{-1}$) and the overall process ($-28.53\ kcal\,mol^{-1}$, Table 1).

As long as the methyl group C9 adopts an equatorial disposition in **INT2**, methyl hydrogen atoms are situated in the acceptor orbital plane. This structure might therefore easily suffer the β-H elimination process leading to the platinahydride species **INT3** (structure **C**, Scheme 2). The transition structure involved in this step, **TS3**, exhibits a clear lengthening of the Pt–C_8 (3.275 Å) and C_9–H (1.174 Å) bonds and shortening of the Pt–H (2.171 Å) and C_8–C_9 (1.437 Å) bonds. Detailed examination of the imaginary frequency mode confirms that the most important geometric change takes place on the H atom between C9 and the metal center.

It can be seen that complete opening of the metallacylopentene in **INT3** takes place by migration of H from C9 (C9–H 1.691 Å) to Pt (Pt–H 1.586 Å). The C8–C9 double bond (1.360 Å) adopts an almost perpendicular disposition with respect to the C6–C7 moiety (dihedral angle −86.8°). It indicates a lack of conjugation between the two multiple bonds, although this destabilizing effect is partially compensated for by a more efficient conjugation with C1–C2 (C1-C2-C6-C7 157.3°). This conformation minimizes the steric hindrance between C9/C10 and both methyl groups at C6 and the catalyst.

Mechanistic studies on transition-metal-catalyzed β-H elimination processes[16] have revealed that they can proceed through four-membered ring intermediate structures[17] in which H coordinates to a metal center by occupying one of the vacant coordination sites before βC–H bond dissociation takes place. Nevertheless, the long Pt···H distance (2.879 Å) suggests that **INT2** should not be a marked β-agostic structure. To gain further insights into this, we located and properly characterized the four-membered ring transition structure involved in this alternative route whereby the C–H bond approaches the Pt (**TS3′**, Scheme S1, see Supporting Information). As expected, it shows the strengthened Pt–C8 (2.137 Å), Pt–H (1.666 Å) and C8–C9 (1.438 Å) bonds and an elongated βC–H (2.226 Å) interaction. IRC analysis confirmed that this transition state directly connects with **INT2**, that is, no β-agostic intermediate was found as a stable structure. Furthermore, the computed energy barrier to reach **TS3′** was very high ($65.86\ kcal\,mol^{-1}$, about $44\ kcal\,mol^{-1}$ higher than the reactant complex), so it must be ruled out as an operative mechanism.

At this point, we have analyzed two possible reaction pathways for the evolution of branch point **INT3** (structure **C**, Scheme 2) to justify the formation of the bicyclic adduct and the absence of the cross-conjugated triene as a reaction product. The first carbocyclization process should proceed through 5-*endo* carboplatination and reductive elimination steps[14] (Scheme 2, path **Ia**) or, alternatively, through intramolecular migratory insertion from a second platinacycle structure (Scheme 2 path **Ib**). Instead, the formation of a conjugated triene in transition-metal catalyzed cyclization of allenynes has been previously reported.[3–5,18] The formal allenic Alder–ene reaction could take place through an analogous route to that proposed for Pt^{II}-catalyzed cycloisomerization of enynes involving a reductive elimination step from the platinahydride intermediate **C** (Scheme 2, path **II**).[13a]

The Alder–ene reaction could therefore take place and yield a cross-conjugated triene from the **INT3** intermediate through the transition state **TS3**-ene. This transition structure reveals that the H approach takes place by closure of the C1–Pt–H bond angle (from 88.4 in **INT3** to 49.1°) and tilted with regard to the π cloud (C2-C1-Pt-H 70.1°) revealing the extensive involvement of the p(π) orbital in the transition state. Finally, IRC analysis indicates that **TS3**-ene leads to the expected triene structure **Prod**-ene. Given the steric hindrance imposed by methyl groups at C6 and C8, we can only observe conjugation between the C1–C2 and C6–C7 multiple bonds (C1-C2-C7-C6 173.4°), which reinforces the η^2-coordination of the terminal olefin to the catalyst. C1–C2 is elongated (1.445 Å) and C2–C7 (1.466 Å), C1–Pt (2.069 Å) and C2–Pt (2.367 Å) are strengthened, as suggested by their bond lengths. The optimized structures for this alternative route are shown in Figure 3. This step is exothermic ($-15.16\ kcal\,mol^{-1}$) and the activation barrier to achieve **TS3**-ene is $18.48\ kcal\,mol^{-1}$, $1.72\ kcal\,mol^{-1}$ less stable than

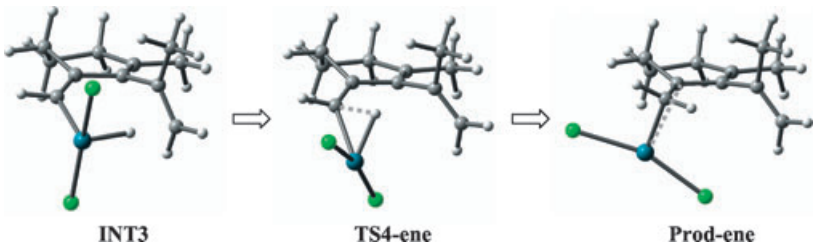

Figure 3. Optimized structures for the alternative Alder–ene reaction of allenyne **9** (path **II**, see Scheme 2).

React. Therefore, the rate-limiting step of the overall process should be the formation of **INT1**.

Alternatively, formation of the carbobicyclic adduct should also take place through Pt^{IV} complex **INT3**. This structure still presents a weak C9–H interaction (1.690 Å), whereas a C1···C9 approximation is required to allow the C–C coupling in a subsequent step. Therefore, we have proposed and properly characterized an additional metal fragment displacement step which takes place through the transition state **TS4a** and yields the intermediate **INT4a** (Scheme 2 path **Ia**, and Figure 4; see also Table S3 in the Supporting Information). The activation barrier for this nearly thermoneutral step (-0.68 kcal mol^{-1}) is 17.91 kcal mol^{-1}, and **TS4a** lies 1.15 kcal mol^{-1} above **React** (Table 1).

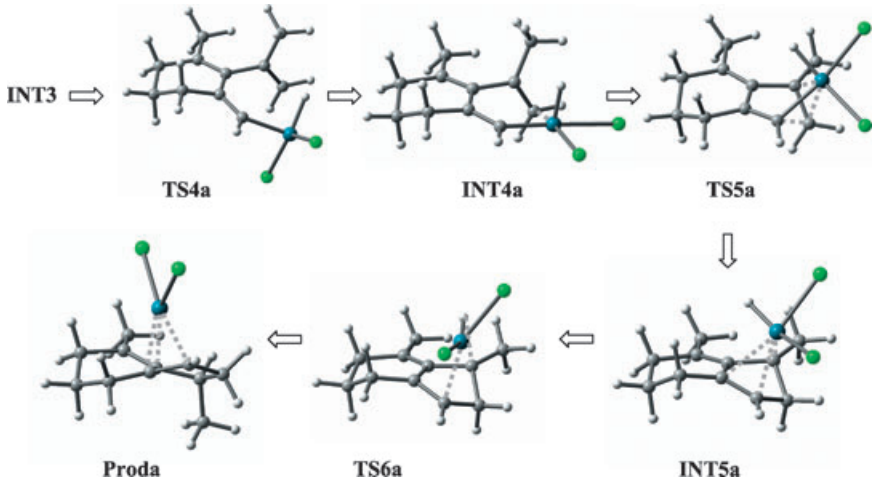

Figure 4. Optimized structures for the mechanistic proposal path **Ia** (see Scheme 2) for the cycloisomerization of allenyne **9**.

The following carbocyclization step would proceed through **TS5a** by intramolecular attack of the nucleophilic alkene carbon C_9 (NPA charge -0.498 in **INT4a**, see Table S4 in the Supporting Information) to the carbene carbon C1 (C1–C9 2.072 Å). Following the intrinsic reaction coordinate, we found the carbobicycle intermediate **INT5a** (structure **D**, Scheme 2), which implies the complete formation of a C1–C9 bond (1.529 Å). In contrast with the previous intermediates, the H atom should occupy one coordination site on the square-planar catalyst framework, implying that a *trans* chloride ligand increases the degree of back-bonding interactions. The computed NPA charges on H confirm this (0.031 in **INT5a** as opposed to 0.155 in **INT3a** and 0.178 in **INT4a**). The 5-*endo* carboplatination step is slightly endothermic (1.30 kcal mol^{-1}) and the activation energy to reach the transition state is rather high (33.33 kcal mol^{-1}, 15.89 kcal mol^{-1} relative to **React**).

Finally, **INT5a** could evolve into the final cycloadduct **Prod** by H-migration from the catalyst to C8 and this reductive step would proceed through the early transition state **TS6a** (C8–H 1.864 Å). It should be noted that this would be an easy transformation as revealed by the low barrier energy computed (2.82 kcal mol^{-1}). It should take place with small geometrical reorganization from **INT5a**, as can be deduced from the geometrical parameters in Table S3 (see Supporting Information). The η^3-coordination of both olefinic moieties to the catalyst in the bicyclo[4.3.0]nonane structure **Prod** (Pt–C1 2.271, Pt–C2 2.140, Pt–C7 2.223 Å) gives rise to a very distorted conjugated diene, with poor conjugation between the multiple bonds (as dihedral angle C1-C2-C7-C6 $-143.5°$ indicates). On other hand, it can be observed that this coordination induces a high stability to the complex.

The calculated results reveal that formation of **INT1** should the rate-limiting step for this mechanistic proposal, and the activation parameters for the overall process show moderate values ($\Delta H_{298}^{\neq} = 15.60$ kcal mol^{-1}, $\Delta S_{298}^{\neq} = 2.65$ kcal mol^{-1} K^{-1}, $\Delta G_{298}^{\neq} = 16.39$ kcal mol^{-1}). It is noteworthy that, **TS5a** lies 0.51 kcal mol^{-1} below **TS1**, an energy difference too small to form a non-ambiguous conclusion about the rate-limiting step.

Interestingly, **TS3-**ene is 14.17 kcal mol^{-1} lower in energy than **TS5a**, which suggests that formation of the conjugated triene should be a process kinetically favored over formation of the bicyclic adduct. This is in sharp disagreement with experimental observations. This result led us to propose an alternative pathway for the evolution of **INT3** into the bicyclic product. According to the proposaed path **Ib** outlined in Scheme 2, **INT3** could afford a second platinacycle intermediate on the PES, **INT4b**, through a H migration from Pt to C8, which then would yield the expected product through an intramolecular migratory insertion step, a common route for the combination of two fragments within the coordination sphere of a metal in numerous transition metal-mediated protocols.

The H migration from the catalyst framework to C8 takes place through the transition state **TS4b** (Figure 5) which depicts the Pt–H elongation (1.892 Å, Table S5, Supporting Information) and the advanced formation of the C–H bond (1.208 Å). Following the reaction coordinate, we located the distorted tetrahedral Pt^{IV} complex **INT4b**, which reveals a six-membered chelate ring structure by the formation of a Pt–C9 bond (2.104 Å). This transformation proceeds with an activation energy of 16.18 kcal mol^{-1} (-0.58 kcal mol^{-1} relative to **React**) and is endothermic (8.98 kcal mol^{-1}). In spite of this metal-induced stepwise H migration from C9 to C8 should proceed through two consecutive endothermic steps, this process yields a reactive intermediate with a proper structure (both carbene and alkyl groups are *cisoi-*

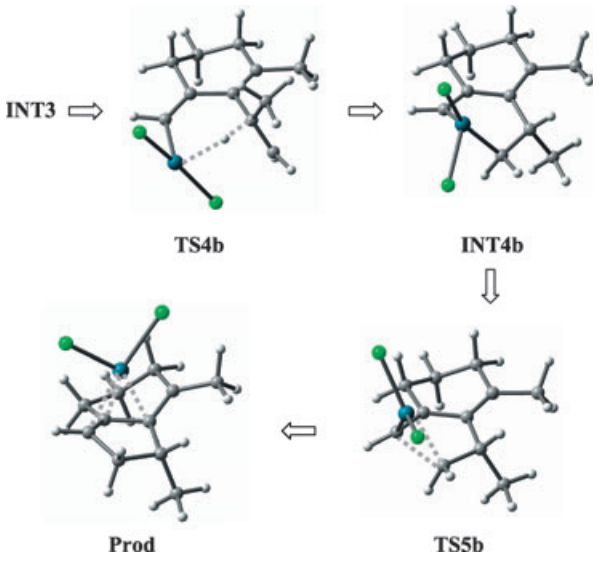

Figure 5. Optimized structures for the mechanistic proposal path **Ib** (see Scheme 2) for the cycloisomerization of allenyne **9**.

dal) to undergo the expected intramolecular migratory insertion.[19] Thus, this step easily affords the bicyclo[4.3.0]nonane ring system through the transition state **TS5b**. This transition structure exhibits the incipient insertion of C9 into σPt–C1 bond (C1–C9 2.164 Å), allowed by the metal framework rearrangement (Cl-Pt-Cl closes to 90.3° and shifts 66.8° from the plane C1-C2-C9). This C–C coupling step is strongly exothermic (−41.63 kcal mol^{-1}) and the activation energy to achieve the transition state is very low (3.74 kcal mol^{-1}). To sum up, this reaction pathway should proceed through five steps, the first being the rate-limiting step. The overall process should be largely favored from a thermodynamic point of view, by −49.42 kcal mol^{-1} (Table 1), and this high value suggests the irreversible character of the catalyzed intramolecular carbocyclization reaction.

According to these results summarized in Figure 6 for comparative purposes, the reaction mechanism path **Ib** would be the preferred pathway for the formation of the bicyclic skeleton and could account for experimental observations concerning the lack of Alder–ene product. As indicated by theoretical results, the kinetically preferred evolution of **INT3** leads to the formation of carbobicycle, whereas the Alder–ene process involves a transition state 2.30 kcal mol^{-1} higher in energy than **TS4b**. Interestingly, the fact that an unsubstituted precursor provides the cross-conjugated triene[14] should rely on the structural properties of **INT3**. Thus, the presence of a substituent on C6 generates a steric demand that prevents efficient π delocalization such that a π cloud for the unconjugated C8–C9 moiety (C6-C7-C8-C9 86.8°) lies in the H-Pt-C1 plane, prone to accept both H and Pt. The absence of a substituent on C6 gives rise to a more conjugated diene by closure of the dihedral angle C6-C7-C8-C9 (55.1°), which implies the unsuitable disposition of the p(π) orbital on the alkene with respect to reaction.

In this context, the value of the dihedral angle C6-C7-C8-C9 in **INT3** provides an interesting clue for the prediction of its evolution.

Experimental data also revealed the equimolecular formation of carbocycles **4** and **5** in the Pt^{II}-mediated cyclization of trisubstituted allenyne **2** (Scheme 1). To gain a better un-

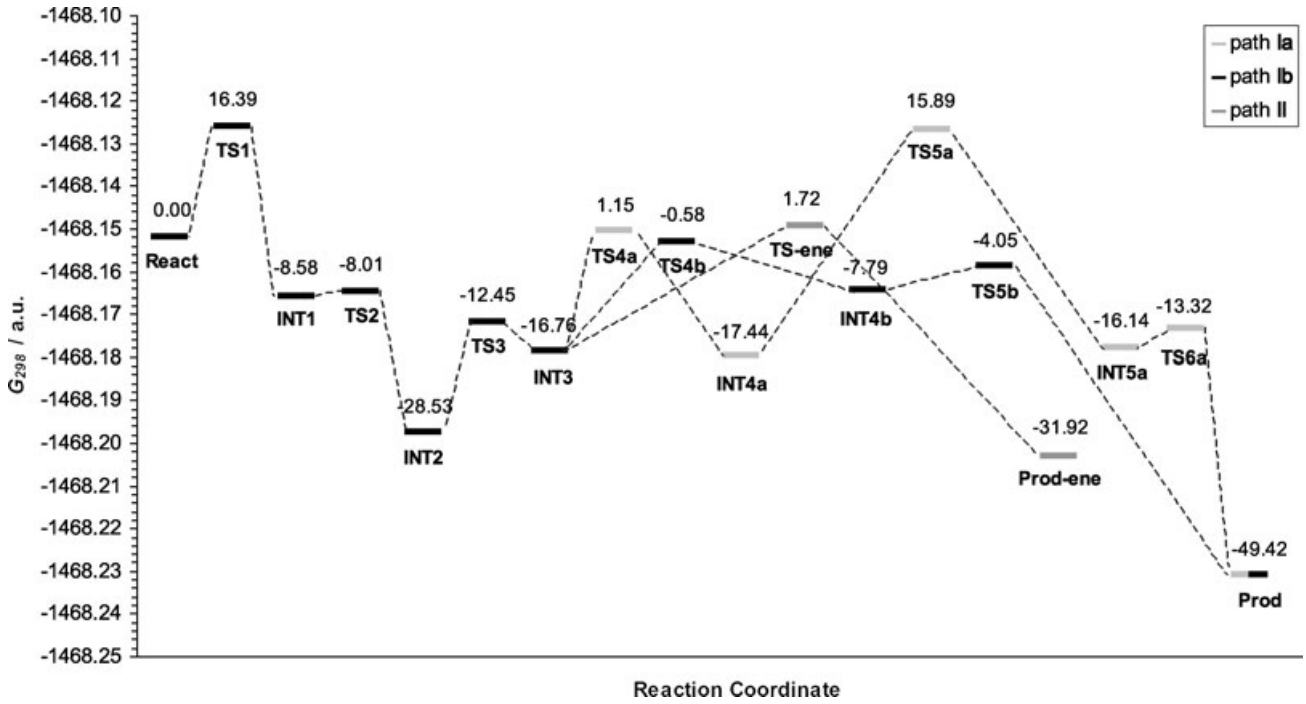

Figure 6. Free energy profile computed for the $PtCl_2$-mediated intramolecular cycloisomerization of **9** (free energy differences relative to reactant complex are given in kcal mol^{-1}).

derstanding about the role of allene substituents on this reaction, we have further analyzed the pattern system **10** as a theoretical model on the basis of the mechanistic scheme previously revealed. The initial coordination of the terminal π bond of allene and alkyne with $PtCl_2$ can give rise to two possible η^4 complexes **React-A** and **React-B**. Both precyclization conformers are predicted to be equally favored, as free energy values reveal (**React-B** is only 0.5 kcal mol^{-1} more stable), since the lack of severe steric interactions between the alkyl group at the terminal allene carbon and the catalyst. Importantly, both structures lead to different intermediates since the terminal methyl substituent C9 can adopt two possible dispositions. This feature has significant consequences in the course of the reaction and it will be discussed in more detail below.

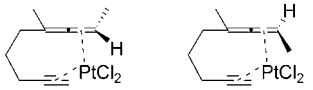

React-A React-B

The cyclometalation step by selective engagement of the external π bond of the allene gives rise to the η^3 complexes **INT1-A** (Figure 7) and **INT1-B** (Figure 9) through the transition states **TS1-A** and **TS1-B**, respectively. The structural parameters and NPA charges of the reactant complexes, transition structures, and intermediate cycloadducts are very similar to those calculated for the tetrasubstituted model (Tables S7 and S8, respectively, see Supporting Information). The main geometrical differences can be found in the shorter Pt–C8 lengths due to the less crowded allene terminal carbon atom. The calculated free energies of activation for conformers **A** and **B** are 16.10 and 16.13 kcal mol^{-1} (Table 2 and Table 3), respectively, which are almost identical (about −0.3 kcal mol^{-1}) to that computed for tetrasubstitued system. Formation of intermediate structures are slightly more exothermic (−11.03 and −13.81 kcal mol^{-1}, for **A** and **B**, respectively) than formation of **INT1** (−8.58 kcal mol^{-1}) due to the lower steric strain, which is more evident for conformer **B** since it lacks steric repulsion between the methyl group at C6 and the terminal allene substituent (C6-C7-C8 123.6° compared to 128.1° in **INT1** and 128.8° in **INT1-A**).

Table 2. Electronic[a] and free[b] energies computed for the $PtCl_2$-catalyzed intramolecular cycloisomerization of **10** (Conformer **A**).

	E[a] [a.u.]	G_{298}[b] [a.u.]	ΔE [kcal mol^{-1}]	ΔG_{298} [kcal mol^{-1}]
React-A	−1428.817614	−1428.861455	0.00	0.00
TS1-A	−1428.792205	−1428.835797	+15.94	+16.10
INT1-A	−1428.836343	−1428.879040	−11.75	−11.03
TS2-A	−1428.836114	−1428.877654	−11.61	−10.16
INT2-A	−1428.868184	−1428.911694	−31.73	−31.53
TS3-A	−1428.826030	−1428.869582	−5.28	−5.10
INT3-A	−1428.836659	−1428.881028	−11.95	−12.28
TS4-A	−1428.817425	−1428.859695	+0.12	+1.10
INT4-A	−1428.838233	−1428.883424	−12.94	−13.79
TS5-A	−1428.828104	−1428.870991	−6.58	−5.98
Prod-A	−1428.898438	−1428.939761	−50.72	−49.14

[a] Includes ZPE correction. [b] Includes thermal corrections at 298 K.

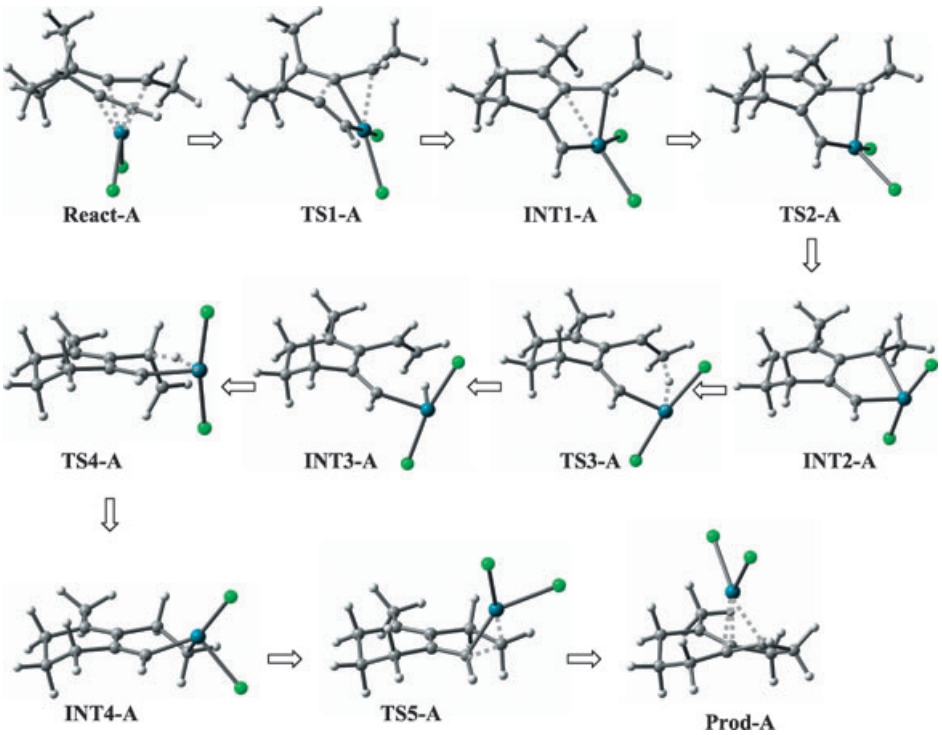

Figure 7. Optimized structures of $PtCl_2$-mediated intramolecular cycloisomerization of **10** (Conformer **A**).

The subsequent isomerization step by a shift of the allyl ligand from its location above the coordination plane leads to the chelate complexes **INT2-A** and **INT2-B**, and takes place through the transition structures **TS2-A** and **TS2-B**, respectively. Likewise, both platina(IV)cycle intermediates show the expected octahedral arrangement of ligands around the d^6 metal, the positions *trans* to the alkyl and σ-alkenyl ligands being vacant. Nevertheless, C9 adopts an equatorial disposition in **INT2-A** and axial in **INT2-B**. Therefore, only conformer **A** presents the right *cis* relationship between the C–Pt and C–H bonds for the β-H elimination. In contrast, conformation **B** inhibits this reaction,

Table 3. Electronic[a] and free[b] energies computed for the $PtCl_2$-catalyzed intramolecular cycloisomerization of **10** (Conformer **B**).

	E[a] [a.u.]	G_{298}[b] [a.u.]	ΔE [kcal mol^{-1}]	ΔG_{298} [kcal mol^{-1}]
React-B	−1428.818461	−1428.862254	0.00	0.00
TS1-B	−1428.793154	−1428.836541	+15.88	+16.13
INT1-B	−1428.841299	−1428.884258	−14.33	−13.81
TS2-B	−1428.792945	−1428.836785	+16.01	+15.98
INT2-B	−1428.838925	−1428.882224	−12.84	−12.53
TS3-B	−1428.829422	−1428.872445	−6.88	−6.39
Prod-B	−1428.884324	−1428.927077	−41.33	−40.68

[a] Includes ZPE correction. [b] Includes thermal corrections at 298 K.

as well as the Alder–ene process, and the allenyne is forced to follow alternative reaction pathways.

Regarding conformer **A**, we have analyzed the analogous structures involved and the free energy surface of the pattern mechanism path **Ib** proposed for tetrasusbstituted allenyne. Structural studies revealed great similarities and the most marked differences arise from the lower congestion around C8. Thus, it facilitates the opening of the Cl_A-Pt-Cl_B bond angle in **INT2-A** (167.7 compared to 162.7° in **INT2**, Table S9, see Supporting Information) and allows a high degree of conjugation between the C6–C7 and C8–C9 moieties in **INT3-A** (as C9–H 2.037 Å and the dihedral angle C6-C7-C8-C9 −63.5 suggest). Regarding distance criteria, β-H elimination proceeds through a later transition state **TS3-A**, as indicated by the Pt–H (2.076 compared to 2.171 Å in **TS3**) and C9–H distances (1.213 compared to 1.174 Å in **TS3**). The Pt–H (1.830 Å (Table S10 (Supporting Information) compared to 1.892 Å in **TS4b**) and C8–H distances (1.251 compared to 1.208 Å in **TS4b**) suggest an earlier transition state, whereas the C1–C9 forming bond length in **TS5-A** (2.142 compared to 2.164 Å in **TS5b**) indicates a slightly later transition structure than for the tetrasubstituted model.

Free energy results show that the β-H elimination step proceeds with a higher activation barrier (Table 2) than for the tetrasubstituted system, as one would expect, due to the lack of the stabilizing inductive effect of an additional methyl substituent at C8. In contrast, the absence of substituents induces less steric strain and a higher stabilization on the intermediate **INT4-A** (−13.79 kcal mol^{-1}, compared to −7.79 kcal mol^{-1} for the tetrasubstituted model). Once again, calculated results indicate that the first cyclometalation is the rate-limiting step, and the overall process is also highly favored from a thermodynamic point of view (−49.14). The optimized structures for this reaction pathway are depicted in Figure 7 and the reaction coordinate is illustrated in Figure 8.

To cover the analysis of the influence of substitution on the terminal carbon atom of the allene, we have further studied the evolution of conformer **B. INT2-B** represents a dead end, but formation of **INT1-B** seems to us necessary on the basis of experimental evidence. We have therefore focused on this intermediate and explored a plausible pathway involving a δ-H elimination and reductive steps. It has been shown that **INT1-B** has square-planar coordination to the metal center in such a way that *cis* chloride ligands are arranged *trans* to the σ-alkenyl and allyl ligands. Interestingly, calculations of frontier molecular orbital energies and coefficients on **INT1-B** reveal that the LUMO+1 acceptor orbital is mainly located on Pt. The orbital shape suggests that an additional ligand (H atom in this case) should approach almost perpendicularly to the plane of the square-planar catalyst framework and occupy an axial position of the octahedral coordination geometry (see Figure S1 in the Supporting Information). Therefore, although orbital analysis supports the fact that α-, β-, and χ-H elimination processes are effectively blocked, we examined the δ-H elimination step. After an extensive computational search, we located and properly characterized the transition state **TS2-B** involving the C–H elongation (1.099 in **INT1-B** compared to 1.692 Å in **TS2-B**, Table S12, see Supporting Information) and $sp^3 \rightarrow sp^2$ rehybridization of C5 from **INT1-B** (C5–C6 1.506 in **INT1-B** compared to 1.430 Å in **TS2-B**).

To facilitate this process, the approach of the catalyst is assisted by the allylic chain, as can be deduced from the ob-

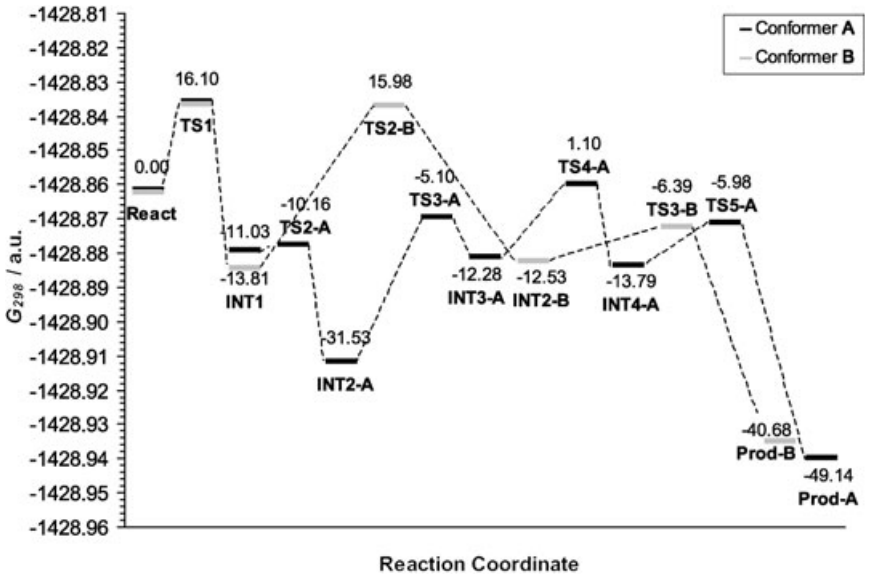

Figure 8. Free energy profile computed for the $PtCl_2$-mediated intramolecular cycloisomerization of **10** (free energy differences relative to reactant complex are given in kcal mol^{-1}).

served strengthening of the Pt–C7 (2.197 Å) and C6–H (1.179 Å) interactions. **TS2-B** leads to the metallacyclopentene **INT2-B**, which resembles an octahedral coordination with a vacant position *trans* to the new σPt–H bond. The platinum center is situated 0.223 Å above the mean-square formed by the four equatorial ligands, with *cis* chloride ligands arranged *trans* to C8 and C1. Interestingly, the five-membered ring is nearly coplanar with the catalyst framework due to the high π conjugation for C1-C2-C7-C8 (dihedral angle −10.6°), as C1–C2 (1.392 Å) and C2–C7 (1.406 Å) bond lengths confirm.

This elementary step is slightly endothermic (1.28 kcal mol^{-1}) and proceeds with a free energy barrier only 0.1 kcal mol^{-1} lower than that of the first step (Table 3), which can be attributed to the distortion required for the proper approximation between reactive centers.

The intermediate **INT2-B** should evolve, by hydrogen migration from the catalyst to C1, to form **Prod-B**. The C1-Pt-H bond angle closes from 89.9° in **INT2-B** to 49.4° in the transition structure involved, **TS3-B**, to allow the catalyst-assisted hydrogen transfer (C1–H 1.596, Pt–H 1.568 Å). As was expected, the H approach takes place with a tilted angle of 96.7° with respect to the alkenyl plane (C2-C1-Pt-H). The C1–H bond has been fully formed in **Prod-B**, which has a η^4-coordinated structure (Pt–C1 2.200, Pt–C2 2.205, Pt–C7 2.204, Pt–C8 2.231 Å).

The elementary step is thermodynamically favored (ΔG_{298} (**INT2-B**→**Prod-B**) = −28.15 kcal mol^{-1}) and proceeds with a low energy barrier (6.14 kcal mol^{-1}), **TS3-B** being 6.39 kcal mol^{-1} more stable than the reactant complex (Table 3). The overall process is highly exothermic (−40.68 kcal mol^{-1}) and, although the H-elimination step involves a rather high-energy transition state, the rate-limiting step in the stepwise pathway is the formation of **INT1-B**. The optimized structures calculated for this reaction pathway are depicted in Figure 9.

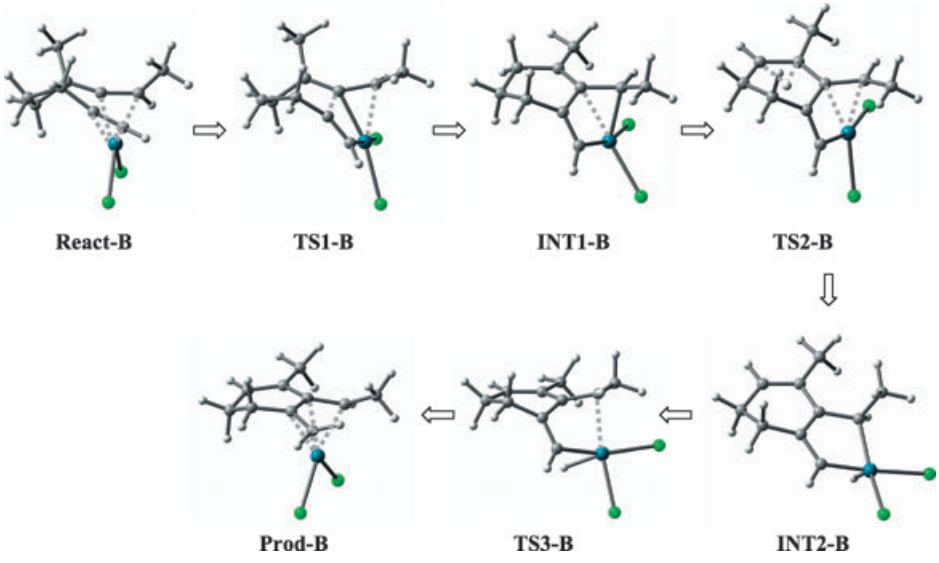

Figure 9. Optimized structures of $PtCl_2$-mediated intramolecular cycloisomerization of **10** (Conformer **B**).

In view of the former results, we observe that only the *Z* isomer can be formed stereoselectively as the triene product, in agreement with experimental data. Therefore, this stereochemical outcome and the alternative formation of the bicyclo[4.3.0]nonane skeleton are merely governed by the conformation of the initial reactant complex.

An energy profile for both catalytic cycles ("**A**" and "**B**") is displayed in Figure 8. Since both reaction pathways show the same rate-limiting step and are highly exothermic, it is reasonable to suppose that $PtCl_2$ treatment of the allenyne precursor should afford both products in comparable yields.

Substitution on the alkyne: The computed results shown above give important information about the general mechanism of the Pt^{II}-catalyzed cyclization of allenynes. However, experimental data reveal that substitution on the alkyne moiety has critical effects on the course of the process. Thus the presence of an alkyl group on the alkyne terminal carbon atom yields unexpected cycloallene systems.[14]

To justify these results, we have considered precursor **11** bearing a methyl group on the alkyne moiety as a model that closely resembled the systems used experimentally, and we have analyzed in detail the structural, electronic and energetic features for the $PtCl_2$-mediated cycloisomerization. As long as a six-membered ring was obtained experimentally (Scheme 1),[14] it is reasonable to suppose that this transformation also involves the intermediacy of a platina(IV)cyclopentene species, formed by selective engagement of the π external bond of the allene through a cyclometalation step. The structural parameters for the reactant complex **React**-Me are very similar to those calculated for the unsubstituted model. The main structural difference results from the steric strain between the catalyst and the methyl group (C11), which induces a weaker Pt–C1 interaction than that for unsubstituted allenyne **9** (2.243 (see Table S13 in the Supporting Information) compared to 2.187 Å for **React**).

From the structural point of view, the transition structure involved in the cylization step **TS1**-Me (Figure 10) is somewhat later than **TS1** as indicated by the shorter C2–C7 bond length (2.081 compared to 2.123 Å for the unsubstituted alkyne). The steric congestion between the methyl substituent and the catalyst is minimized by increasing the C1–C11 (1.489 compared to 1.468 Å in **React**-Me) and Pt–C1 (2.088 Å compared to 2.051 Å in **TS1**) bond lengths. The rest of the geometrical features calculated for the stationary points for this cyclometalation step are indeed very similar to those calculated for the unsubstituted model.

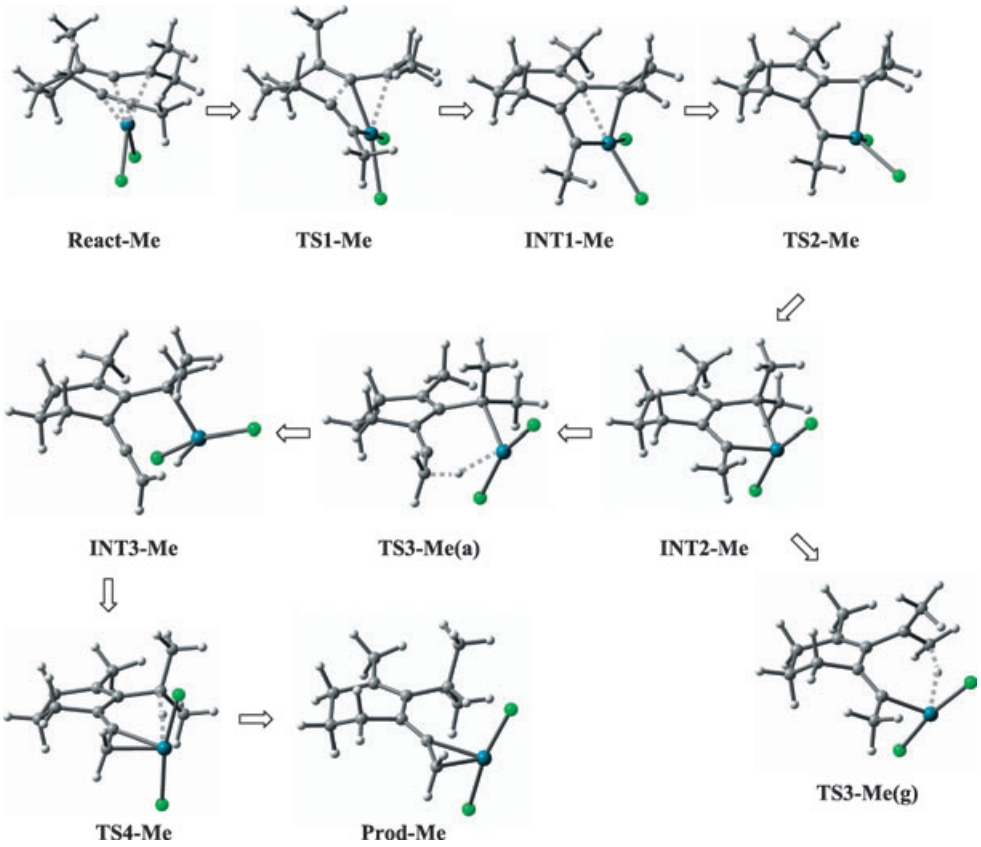

Figure 10. Optimized structures of $PtCl_2$-mediated intramolecular cycloisomerization of **11**.

The free energy of activation is 19.32 kcal mol^{-1} (Table 4), about 3 kcal mol^{-1} higher than that computed for the unsubstituted alkyne, because the transition-state structure becomes more crowded as the bulky alkyne group approachs the allene. Besides steric reasons, the methyl group induces a lower electrophilic character on C2 in the reactant complex (compare Tables S2 and S14, see Supporting Information), which could also account for the higher activation energy although we suppose that it would be a secondary factor. Interestingly, formation of **INT1**-Me is less exothermic (−5.86 kcal mol^{-1}) than formation of the unsubstituted pattern (−8.58 kcal mol^{-1}), a result that can also be attributed to steric effects.

Table 4. Electronic[a] and free[b] energies computed for $PtCl_2$-catalyzed intramolecular cycloisomerization of **11**.

	E[a] [a.u.]	G_{298}[b] [a.u.]	ΔE [kcal mol^{-1}]	ΔG_{298} [kcal mol^{-1}]
React-Me	−1507.408456	−1507.455736	0.00	0.00
TS1-Me	−1507.378205	−1507.424948	+18.98	+19.32
INT1-Me	−1507.419520	−1507.465068	−6.94	−5.86
TS2-Me	−1507.418626	−1507.463811	−6.38	−5.07
INT2-Me	−1507.450580	−1507.496134	−26.43	−25.35
TS3-Me(a)	−1507.425680	−1507.472773	−10.81	−10.69
TS3-Me(g)	−1507.417985	−1507.464359	−5.98	−5.41
INT3-Me	−1507.432991	−1507.480688	−15.40	−15.66
TS4-Me	−1507.426885	−1507.475164	−11.56	−12.19
Prod-Me	−1507.435006	−1507.482702	−16.66	−16.92

[a] Includes ZPE correction. [b] Includes thermal corrections at 298 K.

The isomerization step to the octahedral Pt^{IV}-chelate complex **INT2**-Me proceeds, once again, through the early transition state **TS2**-Me, which implies a very low energy barrier (0.79 kcal mol^{-1}). When comparing the geometries involved in this elementary step and those calculated for the unsubstituted alkyne precursor, no important differences are found.

Intriguingly, both the allylic (at C11) and equatorial *gem*-methyl (at C9) hydrogen atoms are almost situated in the metal coordination plane ($H_{allylic}$ deviates by 8.7° and $H_{gem\text{-}methyl}$ by 9.4° from the plane C1-Pt-C8) in **INT2**-Me, so they are apt to undergo a β-H elimination process. As we have seen for **9**, both the long Pt···$H_{allylic}$ (3.139 Å) and Pt···$H_{gem\text{-}methyl}$ (2.863 Å) distances suggest that **INT2**-Me can not be considered as a β agostic structure. A shorter Pt···$H_{gem\text{-}Methyl}$ distance might promote, indeed, a regioselective elimination from the *gem*-methyl group, in disagreement with experimental results.

The analysis of electronic features reveals that both H atoms also show similar atomic charges ($H_{allylic}$ = 0.256 and $H_{gem\text{-}methyl}$ = 0.262), whereas the exploration of conventional virtual molecular orbitals has not indicated any clear preference for one of them (Figure 11a). In contrast, the alternative natural bond orbital (NBO) analysis[20,21] affords inter-

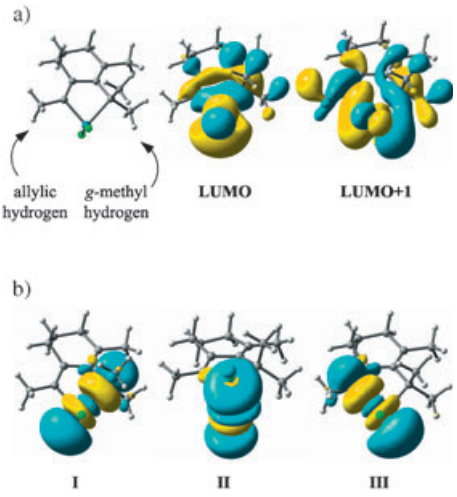

NBO descriptors showing orbital energy (ε), metal atom hybridization (h_M), diatomic symmetry type (σ, π, δ), and occupancy (e) of each of the lowest energy acceptor orbitals.

Acceptor orbital	Energy (a.u.)	Type	h_M	Occupancy (e)
I	-0.07076	σ^*_{CPt}	$sd^{2.28}$	0.2201
II	-0.06174	σ^*_{PtCl}	$sd^{1.64}$	0.5188
III	-0.03398	σ^*_{CPt}	$sd^{2.22}$	0.1992

Figure 11. a) Canonical virtual molecular orbitals LUMO and LUMO+1 computed for **INT2**-Me. b) Shapes and properties of the lowest energy non-Lewis acceptor orbitals for **INT2**-Me.

esting findings for regioselectivity prediction (Figure 11b). NBOs provide a valence bond-type description of the wavefunction, closely linked to classical Lewis structure notions. Whereas the conventional HOMO–LUMO rationale focuses only on the energetic proximity (and then only for symmetry-adapted linear combinations, regardless of the accessibility to a reactive moiety), the NBOs take additional account of spatial proximity and of the asymmetric molecular environment. Shapes and properties of non-Lewis "acceptor" orbitals for the chelate complex **INT2**-Me are shown in Figure 11b. Orbital I, the lowest energy acceptor orbital, clearly suggests that the coordination site *trans* to the alkyl ligand would be the preferred position for accommodating the hydrogen atom in a β-H elimination step. Moreover, a large energy gap is encountered between the acceptor orbital *trans* to alkyl (orbital I) and that *trans* to the alkenyl ligand (orbital III), $\Delta\varepsilon = 0.03678$ a.u. $= 1.0$ eV. Therefore, according to this theoretical approach, the allylic hydrogen atom would be preferentially eliminated.

To gain further insights into this subject, we have computed the activation barrier for both likely processes. First, a β-H elimination from equatorial *gem*-methyl (C9) proceeds through the transition state **TS3**-Me(g). This shows a similar C9–H length (1.178 Å, see Table S15 in the Supporting Information) to that found for the unsubstituted model (1.174 Å), but a moderately reduced Pt–H bond length (2.120 compared to 2.171 Å), due to the steric demand imposed by the substituent at C1. The calculated activation barrier for this elementary step, from **INT2**-Me, rises to 19.94 kcal mol^{-1}, about 4 kcal mol^{-1} higher than that computed for the unsubstituted precursor, due probably to these steric effects. On other hand, a β-H elimination from the allylic group takes place through the transition state **TS3**-Me(a). The opening of the C11-C1-C2 bond angle (from 132.6 in **INT2**-Me to 158.1° in **TS3**-Me(a)) and the shortening of the C1–C11 bond length (from 1.491 to 1.406 Å) indicate that the allene structure is further advanced in the transition state, which alleviates the steric congestion. Amazingly, the activation energy to achieve **TS3**-Me(a) is 14.66 kcal mol^{-1} (−10.69 kcal mol^{-1} relative to **React**-Me), about 5 kcal mol^{-1} lower than that for **TS3**-Me(g).

These results indicate a kinetic regioselective β-H elimination, in agreement with experimental evidence, and qualitatively support the proposal suggested by NBO analysis.

If we compare the intermediates **INT2** and **INT2**-Me, we note that the substituent on C1 forces the opening of the R-C1-C2 bond angle (from 128.9° for the unsubstituted to 132.6° for methyl-substituted precursor) to relieve the steric hindrance between the substituent and C3. Moreover, in both cases the β-H elimination step from C9 proceeds through transition structures where the ring opening implies the opening of the Pt-C1-C2 angle and subsequent closure of the R-C1-C2 bond angle (118.8° in **TS3** for the unsubstituted and 125.6° in **TS3**-Me(g) for the methyl-substituted precursor). This would obstruct this process and could explain, at least in part, the preferred β-H elimination of allylic hydrogen for **11**.

Following the reaction coordinate from **TS3**-Me(a), we located the subsequent local minima **INT3**-Me. The C1–C11 and C2–C1 bond lengths show similar values (1.314 and 1.313 Å, respectively), around that of a typical allene C–C bond.[22] The move of H from Pt towards C8 drives the reaction over to the cyclic vinylallene product (**Prod**-Me) and this final step proceeds through the transition state **TS4**-Me, which involves the lengthening of the Pt–C8 distance (from 2.091 to 3.474 Å) and a shortening of the H···C8 distance (1.452 Å). It is noteworthy that this metal fragment displacement leads to a coordination of the allene moiety to the metal center (Pt–C1 2.076 and Pt–C11 2.121 Å), which should stabilize the transition state. The essentially identical Pt–C1 and Pt–C11 bond lengths (2.065 and 2.083 Å, respectively), and the increased C1–C11 length (1.417 Å) in the product **Prod**-Me imply considerable back donation to the π* orbital of the C1–C11 unsaturated moiety. This structure should therefore be described as a η^2-(allene) complex. Moreover, this effect induces the change of the C2-C1-C11 bond angle to 149.9°.

With regards to energy, this last step proceeds with a low activation energy of 3.47 kcal mol^{-1}, −12.19 kcal mol^{-1} relative to the reactant complex (Table 4), probably due to the previously mentioned coordination of the allene moiety. The overall reaction from **React**-Me to **Prod**-Me is moderately exothermic (−16.92 kcal mol^{-1}), but to a lesser extent than the alternative pathway described above for the unsubstitut-

ed precursors. According to the proposed reaction mechanism the rate-limiting step should be, as for formation of the bicyclic adduct and cross-conjugated triene, the initial cyclometalation process. Figure 12 depicts the calculated free energy profile computed at the B3LYP level for this mechanistic proposal, showing the kinetic preference for β-H elimination from the allylic group, which should account for the observed regioselectivity.

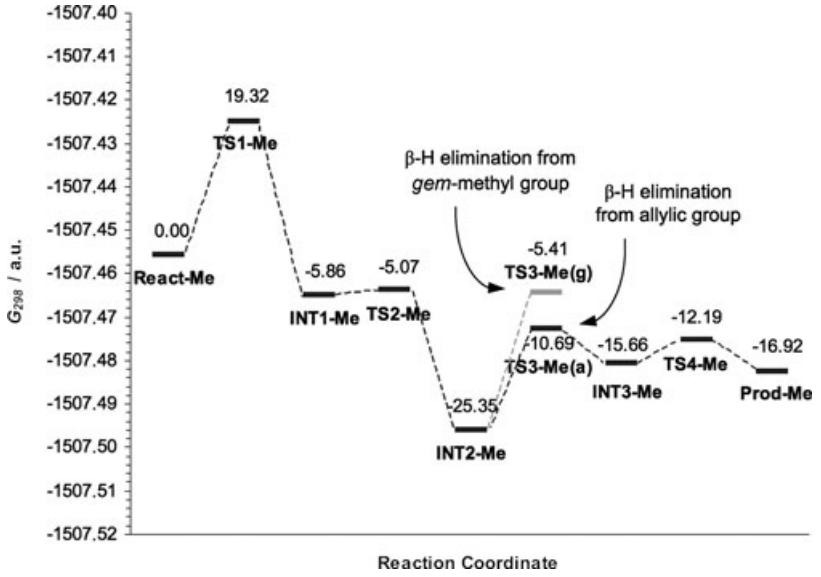

Figure 12. Free energy profile computed for the $PtCl_2$-mediated intramolecular cycloisomerization of **11** (free energy differences relative to reactant complex are inserted in kcal mol^{-1}).

Conclusion

The structurally dependent mechanisms of the $PtCl_2$-catalyzed intramolecular cycloisomerization of allenynes, and the factors governing the involvement of each one, have been investigated for a series of medium-size systems by DFT calculations. Some mechanistic alternatives were tested, and the results allow us to understand and to rationalize the factors that can influence this process.

The mechanistic pathway elucidated for allenyne tetrasubstituted at the allene moiety involves an oxidative cyclometalation process to afford a platina(IV)cyclopentene intermediate. This is followed by a selective β-H elimination from the equatorial methyl group and metal-induced H migration leading to a second octahedral Pt^{IV}-chelate complex. In turn, this would yield the expected bicyclo[4.3.0]nonane ring system through an intramolecular migratory insertion step. Calculations indicate that initial carbocyclization is the rate-limiting step, involving a moderate activation energy, and the overall process is highly exothermic. The possibility of the alternative formal Alder–ene process has also been analyzed, although theoretical results show that this pathway should be less favored from a kinetic point of view, in agreement with experimental results.

The platinum(IV)cyclopentene intermediate formed in the cycloisomerization of allenynes trisubstituted at the allene moiety may evolve through two different pathways. There is a dependence on the orientation of the methyl group at the terminal allene carbon atom, which in turn simply depends upon the conformation of the initial reactant complex. When the methyl group adopts an equatorial disposition, the intermediate progresses through the former mechanistic route involving a β-H elimination step to afford the bicyclic adduct. Conversely, an axial disposition of the methyl group inhibits this reaction and the intermediate is forced to follow an alternative pathway through δ-H elimination and H-migration steps to form a cyclic triene adduct. Moreover, computational results have confirmed the selective formation of the *Z* isomer, again as a consequence of the conformation of the initial reactant complex. Hence, it provides a common origin of the regio- and chemoselectivity observed experimentally.

Precursors bearing a methyl substituent on the alkyne moiety undergo a different process yielding a cyclic vinylallene system. The four-step mechanism determined proceeds through an analogous oxidative cyclometalation route to afford an octahedral Pt^{IV} complex, but this structure undergoes regioselective β-H elimination from the allylic chain. Examination of the natural bond acceptor orbitals of the octahedral intermediate suggests a preference for the allylic rather than for the *gem*-methyl hydrogen atom. Free energy calculations support a regioselective hydrogen elimination providing an interpretation of the experimental results.

In summary, a detailed analysis of the free energy surfaces of the $PtCl_2$-mediated cycloisomerization of allenynes has allowed the characterization of the key steps and the structural, energetic, and electronic implications of the substitution at the allenyne upon the course of these catalyzed reactions. This information provides new insights into the origin of the regio- and chemoselectivities observed, which should help in the development of synthetic strategies and the efficient design of specific or novel unsaturated carbocyclic systems.

Computational Methods

Calculations have been carried out using the Gaussian03 program.[23] The geometries have been fully optimized at the DFT level by means of the B3LYP hybrid functional[24] because of the satisfactory performance of this method in the chemistry of transition metals.[25] Pt has been described by the LANL2DZ basis set,[26] where the innermost electrons are replaced by a relativistic ECP and the 18 valence electrons are explicitly

treated by a double-ζ basis set. For all other atoms, the 6–31G(d,p) basis set has been employed, since polarization functions on hydrogen should be necessary for a better description of the H-elimination processes.

Harmonic frequencies were calculated at the optimization level and the nature of the stationary points was determined in each case according to the number of negative eigenvalues of the Hessian matrix. The intrinsic reaction coordinate (IRC) pathways[27a] from the transition structures have been followed by using a second-order integration method.[27b] This verifies the expected connections of the first-order saddle points with the correct local minima found on the potential energy surface. Zero-point vibration energy (ZPVE) and thermal corrections (at 298 K) to the energy have been estimated based on the frequency calculations at the optimization level, and scaled by the recommended factor.

Natural bond orbital (NBO) analyses[20] have been performed at the DFT level by the module NBO v.3.1[20a] implemented in Gaussian03 to evaluate the NPA atomic charges and NBO descriptors of acceptor orbitals. Molecular orbitals and natural bond orbitals shown throughout this work were contoured at the isovalue 0.02 e au^{-3}.

Acknowledgement

E.S. thanks Prof. Frank A. Weinhold (University of Wisconsin) for helpful discussions.

[1] a) G. C. Lloyd-Jones, *Org. Biomol. Chem.* **2003**, *1*, 215–236; b) C. Nevado, L. Charruault, V. Michelet, C. Nieto-Oberhuber, M. P. Muñoz, M. Méndez, M.-N. Rager, J.-P. Genêt, A. M. Echavarren, *Eur. J. Org. Chem.* **2003**, 706–713; c) E. Mainetti, V. Mouries, L. Fensterbank, M. Malacria, J. Marco-Contelles, *Angew. Chem.* **2002**, *114*, 2236–2239; *Angew. Chem. Int. Ed.* **2002**, *41*, 2132–2135; d) B. M. Trost, F. D. Toste, *J. Am. Chem. Soc.* **2002**, *124*, 5025–5036; e) A. Fürstner, V. Mamane, *J. Org. Chem.* **2002**, *67*, 6264–6267; f) J. W. Dankwardt, *Tetrahedron Lett.* **2001**, *42*, 5809–5812; g) B. Martín-Matute, D. J. Cárdenas, A. M. Echavarren, *Angew. Chem.* **2001**, *113*, 4890–4893; *Angew. Chem. Int. Ed.* **2001**, *40*, 4754–4757; h) A. Fürstner, H. Szillat, F. Stelzer, *J. Am. Chem. Soc.* **2000**, *122*, 6785–6786; i) N. Chatani, K. Kataoka, S. Murai, N. Furokawa, Y. Seki, *J. Am. Chem. Soc.* **1998**, *120*, 9104–9105; j) N. Chatani, N. Furukawa, H. Sakurai, S. Murai, *Organometallics* **1996**, *15*, 901–903.

[2] a) C. Nevado, D. J. Cárdenas, A. Echavarren, *Chem. Eur. J.* **2003**, *9*, 2627–2635; b) M. Méndez, M. P. Muñoz, C. Nevado, D. J. Cárdenas, A. M. Echavarren, *J. Am. Chem. Soc.* **2001**, *123*, 10511–10520.

[3] T. Shibata, Y. Takesue, S. Kadowaki, K. Takagi, *Synlett* **2003**, 268–270.

[4] T. Yamazaki, H. Urabe, F. Sato, *Tetrahedron Lett.* **1998**, *39*, 7333–7336.

[5] D. Llerena, C. Aubert, M. Malacria, *Tetrahedron Lett.* **1996**, *37*, 7027–7030.

[6] C. H. Oh, S. H. Jung, C. Y. Rhim, *Tetrahedron Lett.* **2001**, *42*, 8669–8671.

[7] $[IrCl(CO)(PPh_3)_2]$: T. Shibata, S. Kadowaki, M. Hirase, K. Takagi, *Synlett* **2003**, 573–575.

[8] Rh^I complexes: a) C. Mukai, I. Nomura, S. Kitagaki, *J. Org. Chem.* **2003**, *68*, 1376–1385; b) K. M. Brummond, D. Gao, *Org. Lett.* **2003**, *5*, 3491–3494.

[9] $[Co_2(CO)_8]$: a) B. L. Pagenkopf, D. B. Belanger, D. J. R. O'Mahony, T. Livinghouse, *Synthesis* **2000**, 1009–1019; b) M. Ahmar, C. Locatelli, D. Colombier, B. Cazes, *Tetrahedron Lett.* **1997**, *38*, 5281–5284.

[10] $[Cp_2Ti(CO)_2]$: F. A. Hicks, N. M. Kablaoui, S. L. Buchwald, *J. Am. Chem. Soc.* **1996**, *118*, 9450–9451.

[11] $[Mo(CO)_6]$: J. L. Kent, H. Wan, K. M. Brummond, *Tetrahedron Lett.* **1995**, *36*, 2407–2410.

[12] a) K. M. Brummond, H. Wan, *Tetrahedron Lett.* **1998**, *39*, 931–934; b) K. M. Brummond, H. Wan, J. L. Kent, *J. Org. Chem.* **1998**, *63*, 6535–6545; c) K. M. Brummond, H. Chen, K. D. Fisher, A. D. Kerekes, B. Rickards, P. C. Sill, S. J. Geib, *Org. Lett.* **2002**, *4*, 1931–1934.

[13] a) E. Soriano, P. Ballesteros, J. Marco-Contelles, unpublished results; b) E. Soriano, P. Ballesteros, J. Marco-Contelles, *J. Org. Chem.* **2004**, *69*, 8018–8023.

[14] N. Cadran, K. Cariou, G. Hervé, C. Aubert, L. Fensterbank, M. Malacria, J. Marco-Contelles, *J. Am. Chem. Soc.* **2004**, *126*, 3408–3409.

[15] H. Urabe, T. Takeda, D. Hideura, F. Sato, *J. Am. Chem. Soc.* **1997**, *119*, 11295–11305.

[16] For Group 5, see: a) N. M. Doherty, J. E. Bercaw, *J. Am. Chem. Soc.* **1985**, *107*, 2670–2682; b) B. J. Burger, B. D. Santarsiero, M. S. Trimmer, J. E. Bercaw, *J. Am. Chem. Soc.* **1988**, *110*, 3134–3146; For Pd, see: c) L. H. Shultz, M. Brookhart, *Organometallics* **2001**, *20*, 3975–3982.

[17] a) L. J. Ackerman, M. L. H. Green, J. C. Green, J. E. Bercaw, *Organometallics* **2003**, *22*, 188–194; b) L. H. Shultz, M. Brookhart, *Organometallics* **2001**, *20*, 3975–3982.

[18] K. M. Brummond, H. Chen, P. Sill, L. You, *J. Am. Chem. Soc.* **2002**, *124*, 15186–15187.

[19] For a theoretical work about C–C coupling through intramolecular transition metal-carbene migratory insertion, see: M. A. Iron, J. M. L. Martin, M. E. van der Boom, *J. Am. Chem. Soc.* **2003**, *125*, 13020–13021.

[20] a) E. D. Glendening, A. E. Reed, J. E. Carpenter, F. Weinhold, NBO v. 3.1 implemented in Gaussian03; b) A. E. Reed, F. Weinhold, *J. Chem. Phys.* **1983**, *78*, 4066–4073; c) A. E. Reed, L. A. Curtiss, F. Weinhold, *Chem. Rev.* **1988**, *88*, 899–926.

[21] For extensions of localized bonding concepts to transition metals, see: F. Weinhold, C. R. Landis, *Chem. Educ. Res. Pract. Eur.* **2001**, *2*, 91–104.

[22] Calculations at the B3LYP/6–31G(d,p) level on $H_2C{=}C{=}CH_2$ show a C–C length of 1.307 Å.

[23] Gaussian 03, Revision B.03, M. J. Frisch, G. W. Trucks, H. B. Schlegel, G. E. Scuseria, M. A. Robb, J. R. Cheeseman, J. A. Montgomery, Jr, T. Vreven, K. N. Kudin, J. C. Burant, J. M. Millam, S. S. Iyengar, J. Tomasi, V. Barone, B. Mennucci, M. Cossi, G. Scalmani, N. Rega, G. A. Petersson, H. Nakatsuji, M. Hada, M. Ehara, K. Toyota, R. Fukuda, J. Hasegawa, M. Ishida, T. Nakajima, Y. Honda, O. Kitao, H. Nakai, M. Klene, X. Li, J. E. Knox, H. P. Hratchian, J. B. Cross, C. Adamo, J. Jaramillo, R. Gomperts, R. E. Stratmann, O. Yazyev, A. J. Austin, R. Cammi, C. Pomelli, J. W. Ochterski, P. Y. Ayala, K. Morokuma, G. A. Voth, P. Salvador, J. J. Dannenberg, V. G. Zakrzewski, S. Dapprich, A. D. Daniels, M. C. Strain, O. Farkas, D. K. Malick, A. D. Rabuck, K. Raghavachari, J. B. Foresman, J. V. Ortiz, Q. Cui, A. G. Baboul, S. Clifford, J. Cioslowski, B. B. Stefanov, G. Liu, A. Liashenko, P. Piskorz, I. Komaromi, R. L. Martin, D. J. Fox, T. Keith, M. A. Al-Laham, C. Y. Peng, A. Nanayakkara, M. Challacombe, P. M. W. Gill, B. Johnson, W. Chen, M. W. Wong, C. Gonzalez, J. A. Pople, Gaussian, Inc., Pittsburgh PA, **2003**.

[24] a) C. Lee, W. Yang, R. Parr, *Phys. Rev. B* **1988**, *37*, 785–789; b) A. Becke, *J. Chem. Phys.* **1993**, *98*, 5648–5652.

[25] S. Niu, M. B. Hall, *Chem. Rev.* **2000**, *100*, 353–405.

[26] P. J. Hay, W. R. Wadt, *J. Chem. Phys.* **1985**, *82*, 270–283.

[27] a) K. Fukui, *Acc. Chem. Res.* **1981**, *14*, 363–368; b) C. Gonzalez, H. B. Schlegel, *J. Phys. Chem.* **1990**, *94*, 5523–5527.

Received: June 19, 2004
Published online: December 2, 2004

